

Solar Cycle Variation of 0.3–1.29 MeV/nucleon Heavy Ion Composition during Quiet Times near 1 AU in Solar Cycles 23 and 24

B. L. ALTERMAN ¹, MIHIR I. DESAI ^{1,2}, MAHER A. DAYEH ^{1,2}, GLENN M. MASON ³, AND GEORGE HO ³

¹*Space Science and Engineering
Southwest Research Institute
6220 Culebra Road
San Antonio, TX 78238, USA*

²*Department of Physics and Astronomy
University of Texas at San Antonio
San Antonio, TX 78249, USA*

³*Applied Physics Laboratory
The Johns Hopkins University
Laurel, MD 20723, USA*

(Received May 10, 2023)

Submitted to ApJ

ABSTRACT

We report on the annual variation of quiet-time suprathermal ion composition for C through Fe using Advanced Composition Explorer (ACE)/Ultra-Low Energy Isotope Spectrometer (ULEIS) data over the energy range 0.3 MeV/nuc to 1.28 MeV/nuc from 1998 through 2019, covering solar cycle 23’s rising phase through Solar Cycle 24’s declining phase. Our findings are (1) quiet time suprathermal abundances resemble CIR-associated particles during solar minima; (2) quiet time suprathermals are M/Q fractionated in a manner that is consistent with M/Q fractionation in large gradual solar energetic particle events (GSEP) during solar maxima; and (3) variability within the quiet time suprathermal pool increases as a function of M/Q and is consistent with the analogous variability in GSEP events. From these observations, we infer that quiet time suprathermal ions are remnants of CIRs in solar minima and GSEP events in solar maxima. Coincident with these results, we also unexpectedly show that S behaves like a low FIP ion in the suprathermal regime and therefore drawn from low FIP solar sources.

Keywords: Solar energetic particles (1491) — Suprathermal particles (1491) — Sunspot number (1652)

1. INTRODUCTION

Observations of rare ³He and He⁺ abundances during impulsive solar energetic particle events (Hovestadt et al. 1984b,a; Desai et al. 2006b, ISEP), large gradual solar energetic particle events (Desai & Mason 2001; Mason et al. 1999, GSEP), and co-rotating interaction regions (Chottoo et al. 2000, CIR) have recorded abundances that are several magnitudes in excess of those

observed in the solar wind. Similarly, observations of He⁺ at speeds $2v_{sw}$ have been interpreted as interstellar neutrals that have been ionized in the inner heliosphere and picked-up by the solar wind (Möbius et al. 1995; Feldman et al. 1974; Blum & Fahr 1970; Holzer & Axford 1971; Mason & Gloeckler 2012). Hence they are called “pickup ions”. From these observations, the existence of a seed population with energies between the solar wind and energetic particles (few keV to MeV range; Mason & Gloeckler 2012, and references therein) has been inferred. Since this population has speeds above the bulk solar wind distribution and below energetic par-

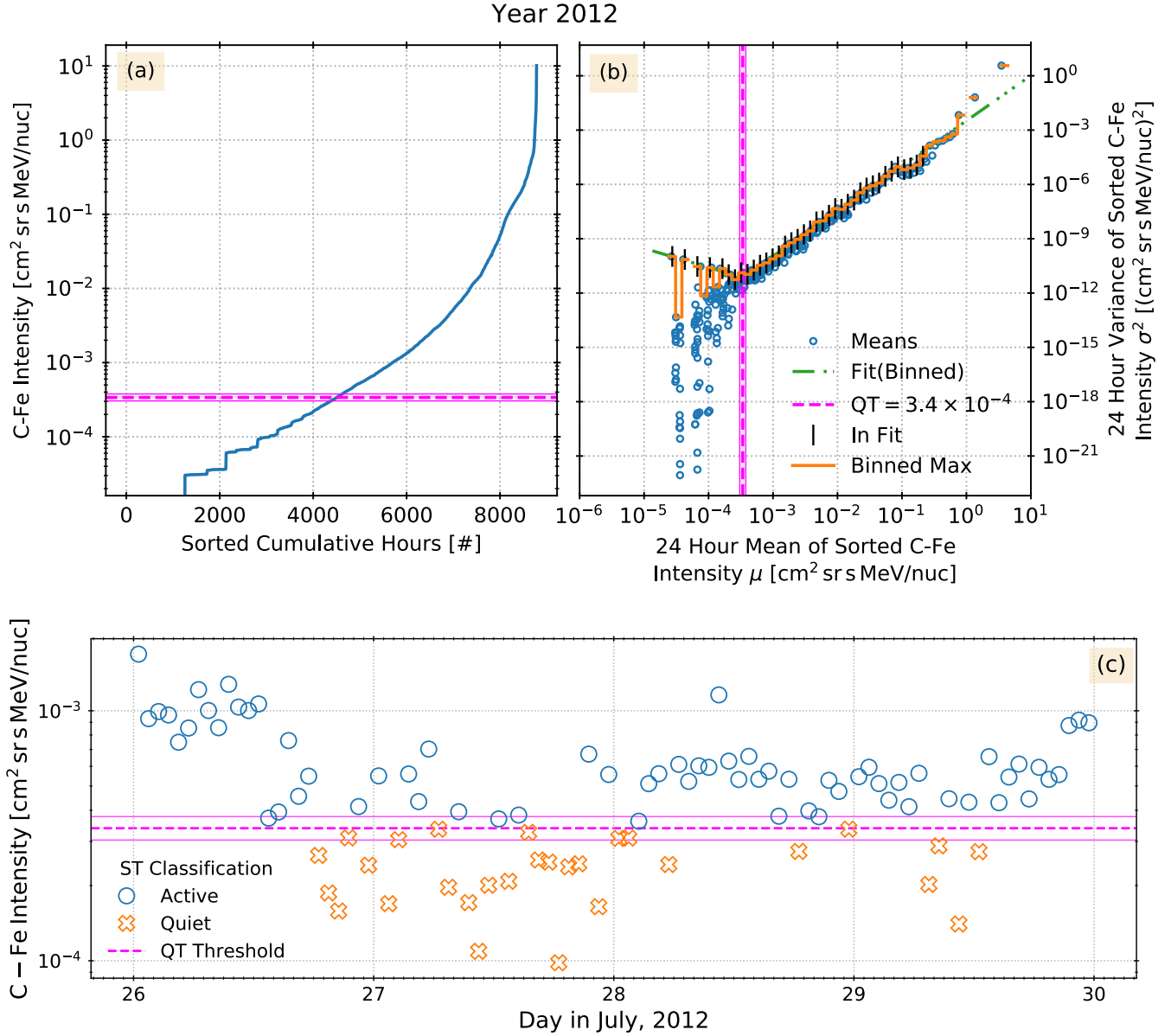


Figure 1. (a) The C to Fe intensity over the energy range 0.11 MeV/nucleon to 1.29 MeV/nucleon. (b) The variance of the C-Fe intensity over 24 hour intervals defined in Panel (a) as a function of the corresponding mean, with the maximum of the 24 hour statistics in a fixed number of bins. A subset is manually selected for fitting with the maximum of two lines. Our quiet time threshold (QT) is the intersection of these two lines and the fits provide a 1σ uncertainty on that value (semi-transparent pink). Data to the left of this threshold corresponds to quiet times. For reference, panel (a) also includes the QT threshold and its 1σ uncertainty; data below the dashed line corresponds to a quiet time. (c) An example of the cumulative C through Fe intensity time series illustrating the difference between active and quiet times. Only 7 of 29 quiet time intervals fall within its 1σ uncertainty.

titles, it is referred to as suprathermal (ST). Additional studies of heavy ions further substantiate these observations (Desai et al. 2003, 2004, 2006b,c,a, 2007; Filwett et al. 2017, 2019). As such, ST ions are a likely seed population accelerated in SEP events. Nevertheless, the mechanism(s) by which the suprathermal energy range is populated remains an open question.

Hypotheses for the source(s) and mechanism(s) by which the suprathermal energy is populated suggest that either ions are accelerated into this energy range by continuous mechanisms including (1) turbulence¹,

¹ Fisk & Gloeckler (2006); Gloeckler et al. (2008); Fisk & Gloeckler (2008, 2012, 2014)

(2) velocity fluctuations², and (3) magnetic reconnection³ or they are remnants of higher energy, discrete processes like (1) coronal mass ejection (CME) driven shocks (GSEP events⁴), (2) impulsive flare events (ISEP events⁵), (3) and CIRs⁶. Desai & Giacalone (2016, Table 2) summarize known sources and acceleration mechanisms.

Observations of quiet times can be identified as the lowest count levels in energetic particle detectors. With such methods Dayeh et al. (2017) showed that the number of quiet hours observed by ACE/ULEIS (Mason et al. 1998) strongly anti-correlates with sunspot number (SSN). Multiple studies have also shown that ST abundances (normalized to oxygen, X/O) resemble solar energetic particle (SEP) events—both impulsive and gradual—in solar maxima and CIRs in solar minima (Desai et al. 2006c; Dayeh et al. 2009, 2017; Zel’dovich et al. 2011, 2018, 2021). That the long term changes in ST ions correlate with SSN likely reflects changes in both the sources from which ST ions are drawn and the acceleration mechanisms associated with these sources (Zel’dovich et al. 2018). Whether or not the accelerating conditions are consistent across solar cycles 23 and 24 is still unresolved (Zel’dovich et al. 2014; Allen et al. 2019).

We study ACE/ULEIS observations from 1998 to 2019 and focus on quiet times. We focus on the energy range 0.3 – 1.28 MeV/nuc, hereafter referred to as suprathermals. Building on Dayeh et al.’s (2017) techniques, we derive annual quiet time intensity thresholds (QT) with an uncertainty or sensitivity metric. With this metric, we characterize the sensitivity of our results to our quiet time selection threshold and verify that it has not introduced systematic bias. We then expand the work of Desai et al. (2006c); Dayeh et al. (2009, 2017) with C, O, and Fe to study the annual behavior of C, N, Ne, Mg, Si, S, Ca, and Fe abundances normalized to oxygen (X/O).

² Fahr et al. (2012)

³ (Drake et al. 2013; Zank et al. 2014)

⁴ Desai & Mason (2001); Desai et al. (2003); Lario et al. (2019); Kahler & Ling (2019); Mewaldt et al. (2012); Jones & Ellison (1991); Zank et al. (2006); Reames (1999); Desai et al. (2006c); Dayeh et al. (2017, 2009) Gradual SEP events originally derive their name from the gradual profile of the associated X-ray events. More recently, the name has become associated with the time profile of the energetic particles associated with the event (Reames 1999).

⁵ Mason et al. (2016, 2002)

⁶ Allen et al. (2019); Mason et al. (2008); Ebert et al. (2012); Fisk & Lee (1980); Richardson (2004); Desai et al. (2006c); Dayeh et al. (2017, 2009); Zel’dovich et al. (2011, 2018, 2021)

The remainder of this paper is organized as follows. Section 2.1 describes our quiet time selection criteria and its uncertainty metric. Section 2.2 discusses the annual number of quiet hours. Section 3.1 presents annual abundances as a function of time. Section 3.2 compares them during solar cycle extrema. Section 3.3 studies M/Q-fractionation of typical ST abundances and how this changes with solar activity. Section 4 examines ST variability as a function of Fe/C along with what this reveals as a function of M/Q and across solar activity. Section 5 discusses our results and Section 6 concludes.

2. QUIET TIME SELECTION AND QUIET HOURS

2.1. Quiet Time Selection

Desai et al. (2006c) define quiet times in ACE/ULEIS and the Wind Suprathermal through Energetic Particle Telescope (STEP) (von Rosenvinge et al. 1995) as intervals with a count threshold below a certain value, irrespective of solar activity. Dayeh et al. (2009, Section 3) build on their work and determine a distinct quiet time threshold for each year by examining the cumulative C through Fe intensity. They found that the lowest 20% to 60% of the intensity values corresponded to quiet times; this percentage depends on the year. Dayeh et al. (2017, Section 2) refined this method, calculating the mean (μ) and variance (σ^2) of this cumulative C-Fe intensity in consecutive 24-hour intervals when the hourly intensity is sorted in increasing order.⁷ By manually inspecting the data, Dayeh et al. (2017) found an inflection point in σ^2 plotted as a function of μ . They determined that intervals with μ less than this inflection point’s correspond to quiet times. We refer to the inflection point as the QT threshold.

Figure 1 Panels (a) and (b) plot ACE/ULEIS data over the energy range 0.11 MeV/nucleon to 1.29 MeV/nucleon from 2012 in Dayeh et al.’s (2017) manner. Panel (a) plots the cumulative C-Fe hourly intensity during 2012 in ascending order. Panel (b) bins the data in Panel (a) into 24-hour intervals and calculates each bin’s mean (μ) and variance (σ^2), plotting $\sigma^2(\mu)$. Panel (b)’s pink vertical line is the inflection point. Because Dayeh et al.’s (2017) thresholds were manually set, determining the sensitivity of this analysis’ results to the choice of inflection point becomes arbitrary and their selection criteria remains *ad hoc*.

We build on Dayeh et al.’s (2017) method, identifying this QT threshold using non-linear fitting. Along with the QT threshold, our method provides an uncer-

⁷ These intervals do not correspond to chronological days, but rather consecutive 24-hour periods when the data is sorted as described.

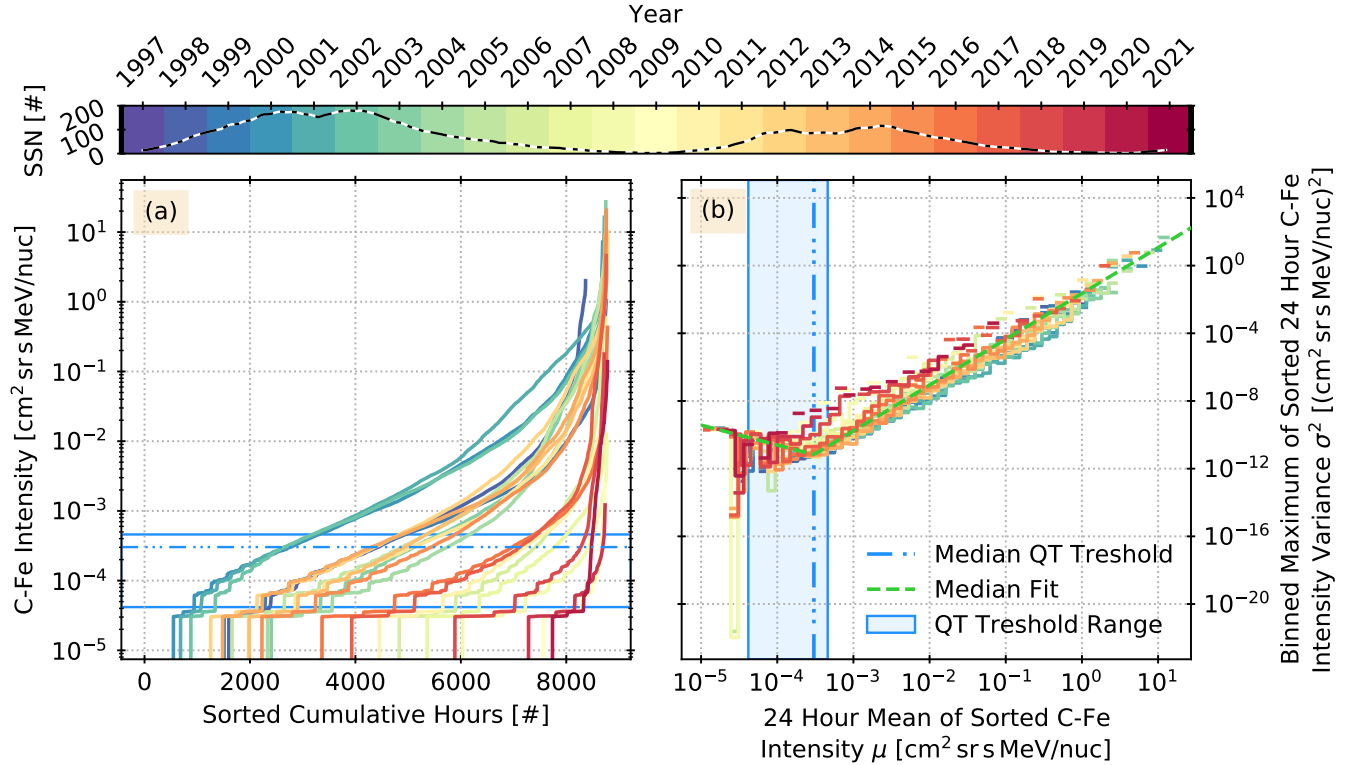


Figure 2. A summary of the QT selection fits per Figure 1 across all years. The color bar identifies the year corresponding to each line, with the 13-month smoothed SSN over plotted for context. Panels match Figure 1. Panel (b) shows the binned maxima and a summary of the fits across all years. The QT threshold region on the left panel is completely transparent for visual clarity.

tainty metric, which allows us to quantify the sensitivity of our analysis to the selection of quiet times. We start by generating plots of $\sigma^2(\mu)$ for each year in the manner of Figure 1. We have binned σ^2 in a fixed number of logarithmically-spaced μ -intervals and calculated the maximum in each bin plotted as a solid orange line. For 2018, there are 54 bins, 62 for 2019 and 2020, and 72 otherwise. We then select a subset of these binned values indicated with vertical black dashes and fit them in log-space with the maximum

$$\text{QT}(\mu) = \max(\sigma_1^2, \sigma_2^2) \quad (1)$$

of two power laws

$$\sigma^2(\mu) = \sigma_0^2 \mu^\epsilon \quad (2)$$

subject to the condition that the power laws σ_1^2 and σ_2^2 are equal at the quiet time threshold QT

$$\sigma_1^2(\text{QT}) = \sigma_2^2(\text{QT}). \quad (3)$$

In effect, this method balances the weight given to the data below and above the inflection point so that we can properly identify the change in slope corresponding to the QT threshold. The 1σ fit uncertainty for the QT

threshold is then the interval over which we can test the sensitivity of our results. That being said, because quiet times inherently involve small numbers, we chose to use the interval $\text{QT} \pm 1.25\sigma$ to provide additional confidence that our fitting methods do not inadvertently include active periods that will dominate our statistics. Figure 1 plots this 1σ fit uncertainty on the QT threshold as a semi-transparent, pink band. Panel (c) plots an example time series of the cumulative C through Fe intensity during July, 2012. The QT threshold shows that only 7 of 29 quiet time intervals fall within QT's 1σ uncertainty.

Figure 2 summarizes the QT threshold for all years. Panel (a) plots the data from all years in the same manner as Figure 1. Panel (b) plots the binned values from all years. These correspond to the orange line in Figure 1 (b). In both panels, the color bar identifies the year corresponding to each line. While later analysis utilizes the annual SSN, we over plot the higher time resolution 13-month smoothed SSN (dash-dotted line) on the color bar to provide a time reference instead of the annual SSN. In Panel (b), the vertical blue dashed-dotted line is the median QT threshold. A semi-transparent blue band indicates the range of QT thresholds. The median

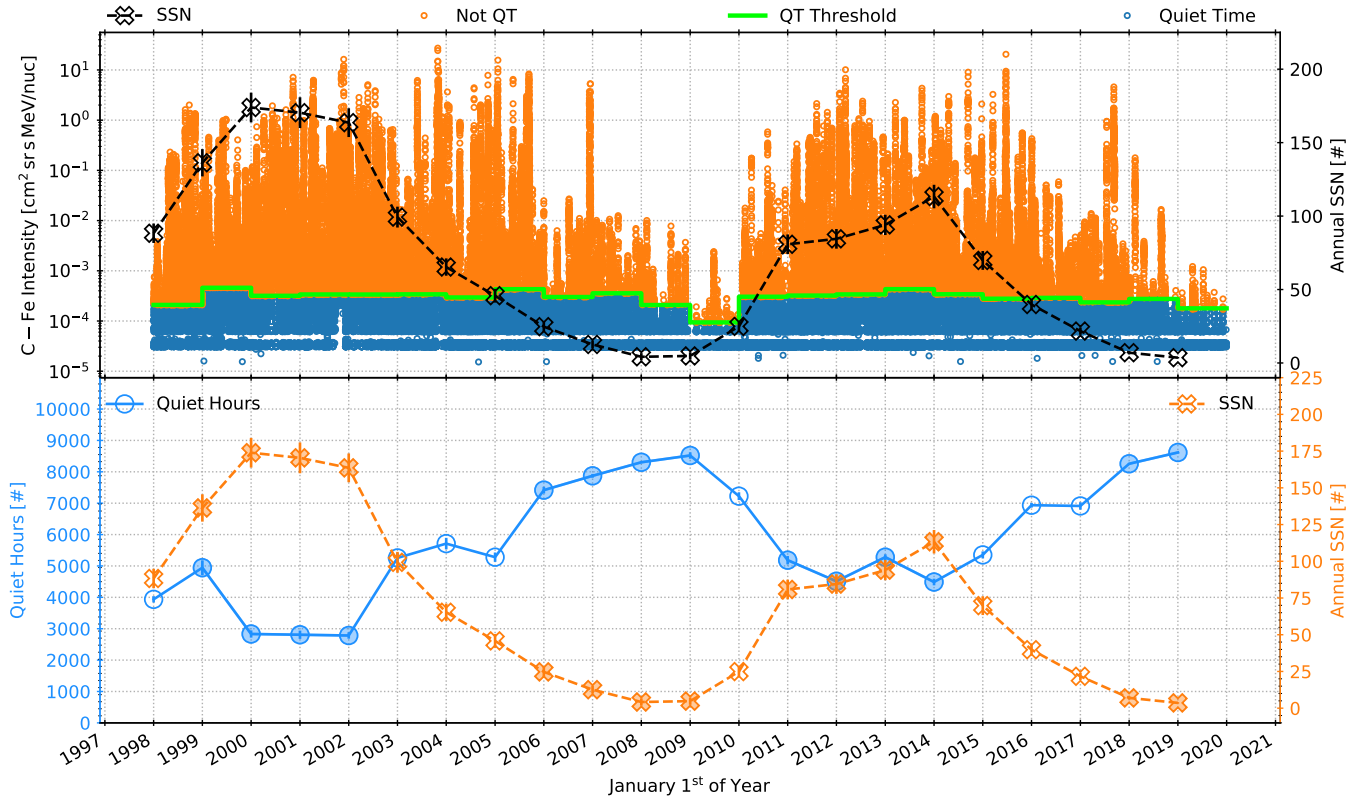


Figure 3. (a) Hourly C–Fe intensity as a function of time. (b) The left axis plots the annual number of quiet hours. The right axis in both panels plots annual SSN. In the bottom panel, partially filled markers indicate years corresponding to solar cycle extrema, as defined in Section 3.2.

of all fit parameters indicates the typical fit in dashed green. All SSN data is provided by the Solar Information Data Center (SILSO World Data Center 2020; Vanlommel et al. 2005, SIDC).

2.2. Quiet Hours

Figure 3 (a) plots hourly C–Fe intensities over the energy range 0.3 MeV/nuc to 1.29 MeV/nuc as a function of time. The QT threshold (solid green) divides quiet time intensities (blue) from other intensities (orange). Panel (b) plots the number of quiet hours (blue circles) as a function of time; error bars are described below. Both panel’s right axis plots the annual average SSN (“X”); error bars are the standard deviations provided by SIDC. The Pearson correlation coefficient $\rho = 0.51$ between the QT threshold and SSN indicates that the QT threshold is moderately tied to changes in SSN. In contrast, the number of quiet hours strongly anti-correlates with annual SSN at the $\rho = -0.95$ level.

To quantify the sensitivity of our results to the QT threshold selected, we have calculated 21 logarithmically spaced steps centered on QT over the range $\pm 1.25\sigma$, where σ is the QT threshold fit uncertainty from Figure 1. We use 1.25σ to provide additional confidence in

the applicability of our method and robustness of our results. In both panels, we plot the standard deviation of the QT threshold across this $\pm 1.25\sigma$ range as error bars, which are typically smaller than the markers.

Abundance X/O	Correlation Coefficient
C	−0.84
N	−0.06
Ne	−0.40
Mg	+0.90
Si	+0.89
S	+0.91
Ca	+0.81
Fe	+0.89

Table 1. Correlation coefficients for indicated abundances (X/O) with annual SSN $\rho(X/O, \text{SSN})$ from Figure 4.

3. ANNUAL ABUNDANCES OVER TIME AND DURING CYCLE EXTREMA

3.1. Annual Abundances Over Time

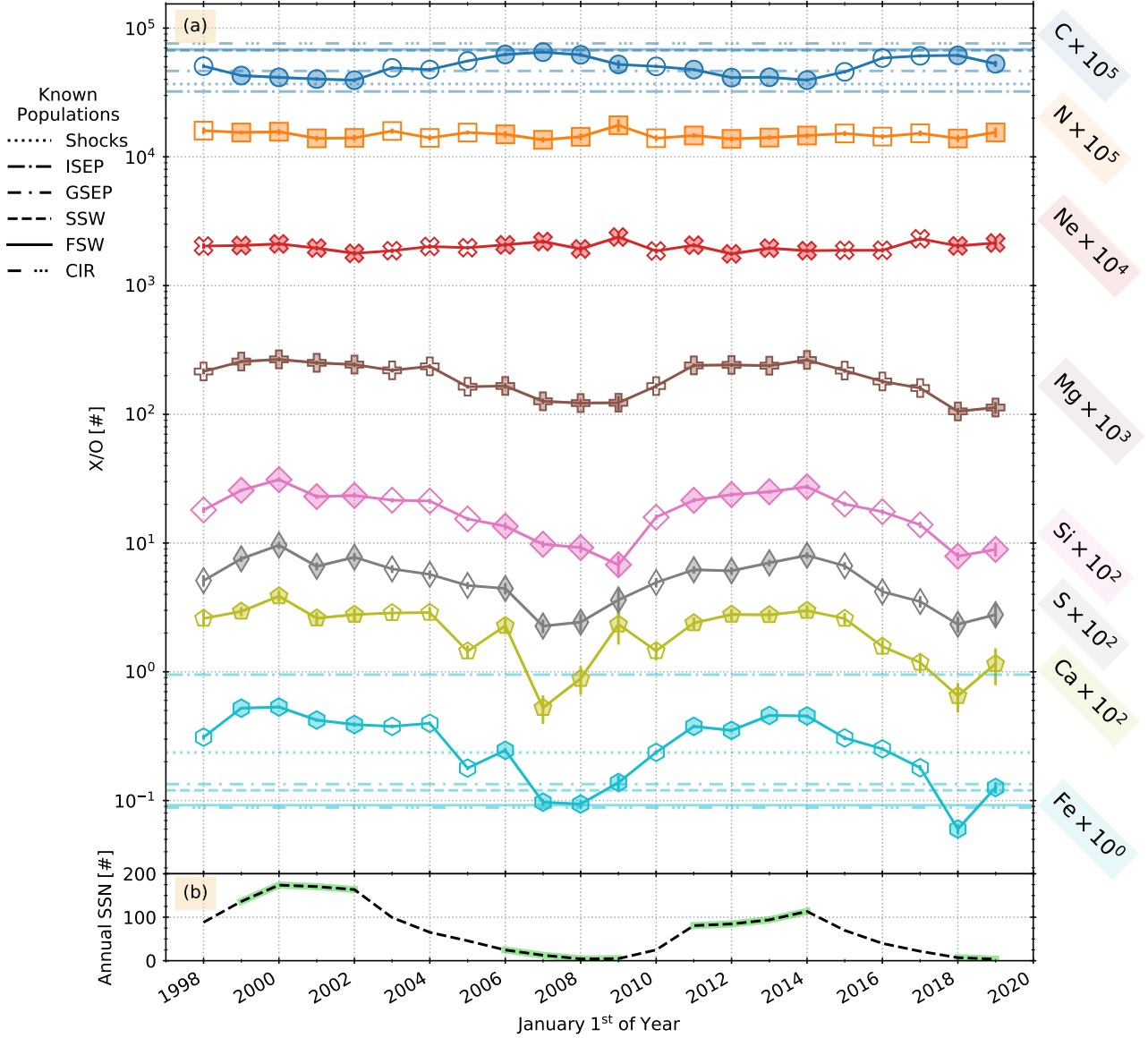


Figure 4. (a) Annual quiet time abundance normalized to oxygen (X/O). Each species X is labeled on the right hand side of the plot and scaled by the indicated value. Horizontal lines indicate typical C and Fe abundances for events indicated in the *Known Populations* legend. (b) Annual SSN, with solar cycle extrema years highlighted in green. As in Figure 3, X/O data occurring during solar cycle extrema are partially filled. Table 1 gives the signed correlation of each abundance with SSN $\rho(X/O, SSN)$.

Figure 4 Panel (a) plots the annual abundance of quiet time C, N, Ne, Mg, Si, S, Ca, and Fe with respect to oxygen (X/O) in the energy range 0.3 MeV/nuc to 1.29 MeV/nuc from 1998 through 2019. Each species is identified by a label on the right side of the plot and shifted vertically by the indicated value (e.g. C by 10^5). As with the intensities in Figure 2, these abundances account for and include intervals with zero particle counts. Error bars indicating the propagated uncertainty of each X/O are typically smaller than the markers. Excluding Fe in 2004 and 2010, the variability as a function of

QT $\pm 1.25\sigma$ range is smaller than the propagated uncertainty and therefore not shown.

Figure 4 (b) plots the annual SSN. Table 1 gives the correlation coefficient between X/O and SSN, $\rho(X/O, SSN)$. In general, C, N, and Ne abundances anti-correlate with SSN and the others positively correlate with it. However, only the positive correlations and Carbon's anti-correlation are strong ($|\rho| > 0.6$). Section 5.4 discusses the relationship between ρ and ion M/Q.

Following Desai et al. (2006a), Table 2 lists a series of known abundances from a variety of sources and cites the sources for each of these population. It also includes average abundances from solar minima and maxima, calculated with this paper’s data. Horizontal lines in Figure 4 indicate representative values of C/O and Fe/O from the following subset of known populations:

- interplanetary shocks (Shocks),
- slow solar wind (SSW),
- fast solar wind (FSW),
- gradual solar energetic particle (SEP) events (GSEP),
- impulsive SEP events (ISEP), and
- co-rotating interaction regions (CIR).

Table 4 contains the data in Panel (a).

3.2. Abundances During Solar Cycle Extrema M/Q

ST ions are likely associated with CIRs in solar minima (Desai et al. 2006c; Dayeh et al. 2009, 2017; Zel’dovich et al. 2011, 2018, 2021). CIRs are formed when coronating fast solar wind streams from coronal holes overtake slow wind streams. In the outer heliosphere and occasionally at 1 AU, the boundaries of CIRs steepen into forward and reverse shocks. Solar wind abundances are governed by their associated sources on the Sun’s surface. Solar sources along with the occurrence rate of flares and CMEs (Webb & Howard 1994) change with the solar activity cycle. Alterman et al. (2021) showed that the solar cycle driving solar wind abundances changes ~ 250 days prior to sunspot minima, likely due to changes in the solar magnetic field that impact solar source regions (McIntosh et al. 2014; McIntosh & Leamon 2017; McIntosh et al. 2015).

To compare abundances across solar cycle extrema, we follow Zhao et al. (2013) and select time periods around each extremum based on the normalized SSN (NSSN). NSSN is the SSN in each solar cycle normalized to that cycle’s maximum SSN. This feature scaling accounts for SSN’s variable amplitude and transforms it into an amplitude-independent clock. Allen et al. (2019) used a similar method to assign CIRs to solar cycle extrema. The years we consider to have abundances representative of solar minima have an annual NSSN ≤ 0.15 . Years with abundances representative of solar maxima correspond to NSSN ≥ 0.7 . This corresponds to approximately 4 years per extrema and, during years representative of solar minima, primarily selects those from the declining phase of solar activity. Figure 4 highlights solar cycle extrema in the bottom panel and partially shades the corresponding X/O data points. Later sections use these intervals to compare ST properties during solar cycle extrema. By biasing our solar minima

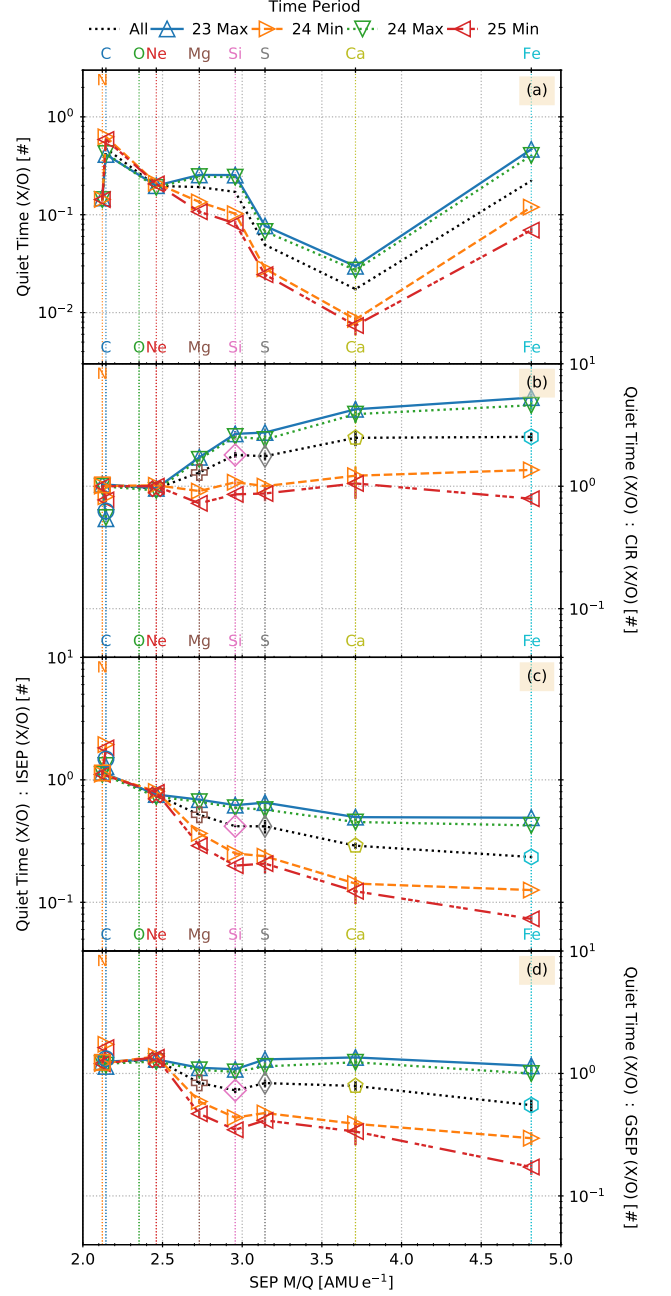


Figure 5. (a) Annual quiet time abundance X/O along with these abundances normalized to its known reference abundances in (a) CIRs, (b) ISEP, (c) GSEP events as a function of GSEP M/Q for all years along with solar cycle extrema indicated in the legend. Each species is identified on the top axis.

selection to the declining phase of solar activity, we ensure that our Minima 24 and 25 intervals are weighted toward ST ions that are generated by a single solar cycle, not an admixture of two (Alterman et al. 2021; McIntosh et al. 2014; McIntosh & Leamon 2017; McIntosh et al. 2015).

3.3. Abundances as a Function of M/Q

Figure 5 (a) plots X/O during solar cycle extrema as a function of GSEP M/Q . We use the same average GSEP charge states as Section 5.2 of Desai et al. (2006a). Each element’s symbol is indicated on the top axis. As expected from Figure 4, variability of any single data point with the threshold selected in Section 2.1 is smaller than the statistical uncertainty associated with that data point. The plot shows a clear trend with increasing M/Q : the abundances decrease from C to Ca, but Mg and Si lie above this line. The abundances then increase from Ca to Fe. During both solar cycle extrema, Fe/O is more similar to Mg/O and Si/O than S/O or Ca/O. The trend for solar maxima-representative abundances in Panel (a) is also qualitatively similar to 0.14, 1.1, and 10 MeV/nuc ions reported by Mewaldt (2001, Fig. 6).

ST ions likely suffuse the heliosphere (Tsurutani & Lin 1985; Desai et al. 2003; Wiedenbeck et al. 2003). They are variously associated with CIRs (Chottoo et al. 2000), ISEPs (Hovestadt et al. 1984b,a; Desai et al. 2006b), and GSEPs (Desai & Mason 2001; Mason et al. 1999), depending on the phase of solar activity. In particular, prior observations suggest that CIRs are the dominant source of ST ions during solar minima (Desai et al. 2006c; Dayeh et al. 2009, 2017; Zel’dovich et al. 2011, 2018, 2021) and both ISEP and GSEP events dominate ST sources during solar maxima (Dayeh et al. 2017, 2009; Desai et al. 2006c). To quantify the similarity of suprathermal abundances to the known populations in Table 2, we have generated plots of quiet time X/O normalized to them Quiet Time (X/O) : Known (X/O) as a function of M/Q , averaging over each solar cycle extremum and all years from Figure 3. Panel (b) plots the CIR case. With the exception of carbon, all suprathermal abundances resemble their CIR abundance in solar minima. Given that C is known to be enhanced in CIRs and the solar wind with respect to the photosphere and corona (von Steiger et al. 2000; Lodders 2003; Feldman & Widing 2003; Mason et al. 1997), this is not unexpected (Desai et al. 2006c; Dayeh et al. 2009, 2017). Panels (c) and (d) plot X/O normalized to representative ISEP and GSEP abundances, respectively. During solar maxima, normalizing quiet time X/O to the representative ISEP does not remove the M/Q trend, but normalizing to the GSEP abundances does.

4. ABUNDANCES AS A FUNCTION OF Fe/C

To characterize the variability of ST abundances, Figure 6 plots each species’ abundance X/O as a function of Fe/C. We follow Reames et al. (1994); Mason et al. (2004) and take, “Fe/C as the most sensitive indicator

of the general enrichment of heavier elements relative to lighter ones.” (Reames et al. 1994) Data points and connecting line colors correspond to the year of observation. Marker shapes for each species match prior figures and they are connected to aid the eye. Species are indicated as in Figure 4. Propagated error on the abundances is, excluding Ca, at most the marker size and all are excluded from the plot for visual clarity. Dash-dotted lines are power law fits to the data. Blue boxes indicate the range of values corresponding to each solar cycle extrema. In general, these trends show cyclic behavior with lower Fe/C and the correlated X/O values during solar minima and the higher Fe/C values during solar maxima. Unlike ^3He in ISEP events (Mason et al. 2004), these ST observations are not uniformly distributed with $\ln(\text{Fe}/\text{C})$, but rather show a large spread during solar minima and a concentration during solar maxima. These slopes are consistent with the trends in Figure 4 and, as can be inferred from Figure 4, C/O is the exception to this trend showing an anti-correlation. Ca/O is the most significant example, showing a weak gradient during solar maximum and periods of high Fe/C.

Figure 7 plots the power law exponents derived in the same manner as Figure 6 for (a) each solar cycle extremum as a function of time along with (b) all the data. Individual plots for deriving each slope in panel (a) are not shown for lack of space. The data are plotted at the value corresponding to the QT threshold derived in Section 2 and error bars representing the sensitivity to the QT threshold’s uncertainty are typically smaller than the markers. Excluding Ca along with possibly S and Ne, the power law exponents b are roughly consistent across the cases plotted. C has the smallest exponent of -0.21 and Fe the largest 0.79. In contrast to the possibly cyclic variation of that most species’ exponents demonstrate with solar activity, Ne and S both decrease from solar Maximum 23 to Minimum 25. However, more than four solar cycle extrema are required to determine if this difference is due to random fluctuations or is indicative of a true difference between these species and the rest of those studied. The large change in Ca’s slopes are due to a flattening of Ca/O during solar maxima observed in Figure 6, which drives these slopes down. While C, N, Mg, & Fe show some consistent variability from solar minima to maxima, the power law exponents are markedly more consistent and show less overall variation across cycle extrema.

To characterize the variability of quiet time ST ions studied in this paper as a function of mass-per-charge, Figure 8 plots these exponents as a function of M/Q . In general, the slopes increase with M/Q , implying that larger M/Q quiet time ST ions have a more variable

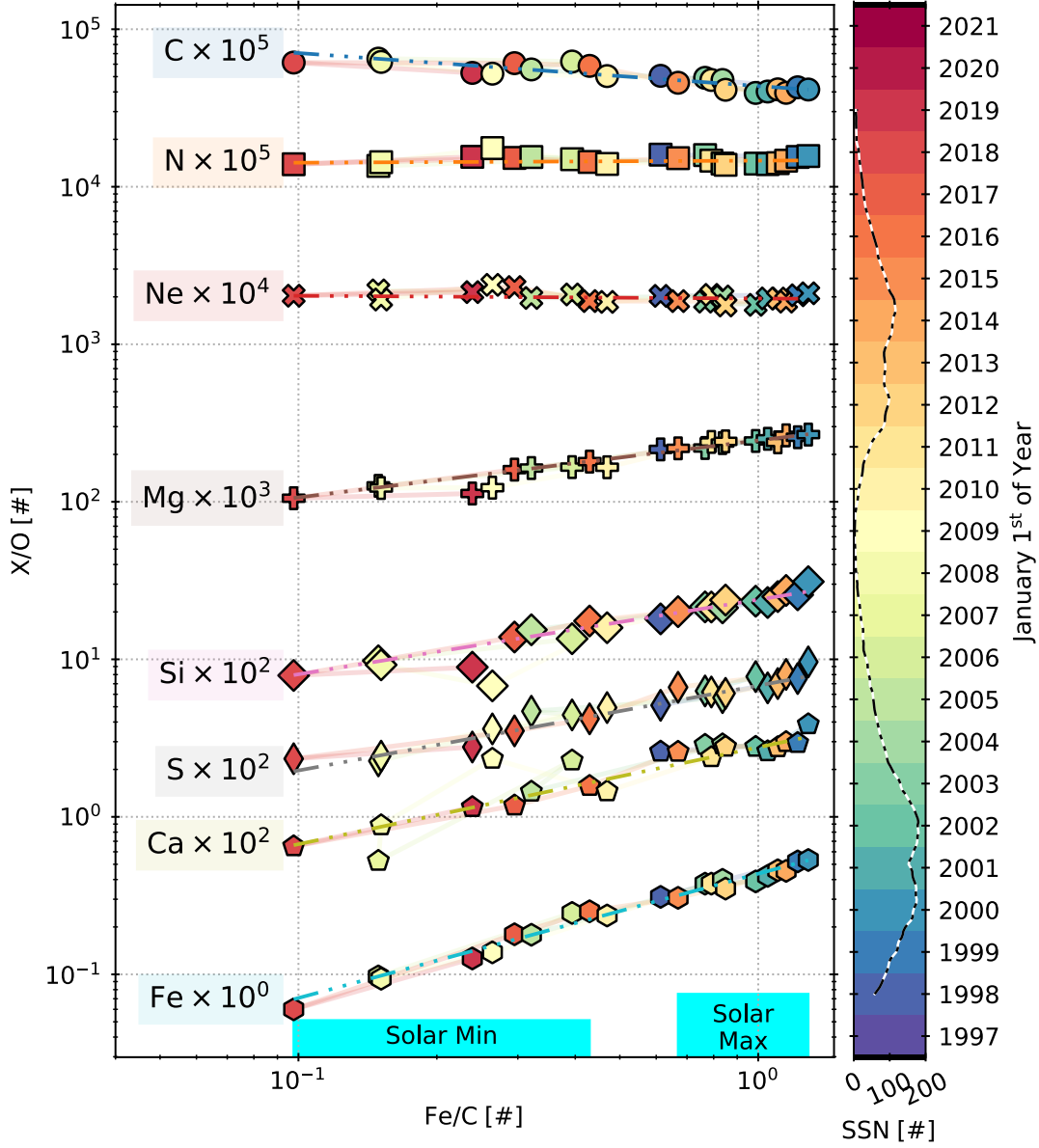


Figure 6. The annual abundance X/O as a function of Fe/C . Markers and the connecting segments are colored according to their year; segments are partially transparent. A power law is fit to each X/O as a function of Fe/C and plotted in the color matching the adjacent label box and Figure 4.

enrichment pattern across the solar cycle. During solar maxima, Ca outliers are likely due to the flattening noted in Figure 6. Broadly, there may also be a change in the variability trend at S, where the change in slopes is steeper for $M/Q < M/Q(S)$ and shallower otherwise. To characterize the general nature of this trend, we have fit the data in Figure 8 with a line, reserving more detailed analysis for future study. We have also plotted the trend from Desai et al. (2006a, Fig. 15) for GSEP event at 0.38 MeV/nuc. Broadly, the trends during solar maxima are consistent with the GSEP trend.

Figure 9 plots the fractionation slopes from Figure 8 (a) across solar cycle extrema and (b) for all data. Here, we plot the value corresponding to the threshold derived in Section 2 with its fit uncertainty with dotted blue error bars and variability with QT variability with solid orange error bars. The variability error bars are calculated as in Section 2.2. D06 is the slope from Desai et al. (2006a, Fig. 15). Two observations stand out. (1) The fit uncertainty is markedly larger than the variability of our results due to QT threshold selection. (2) The horizontal line from Desai et al. (2006a) (nearly) intersects the *Fit* error bars for all four solar cycle extrema.

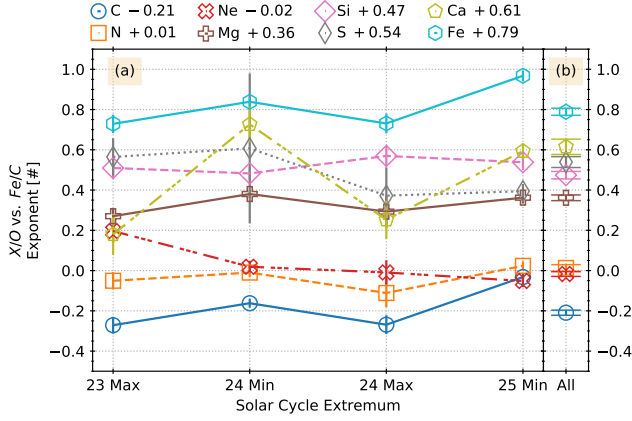


Figure 7. Power law exponents from fits to $X/O(\text{Fe}/\text{C})$. Panel (a) plots data derived from Figure 6 for subsets of the data corresponding to solar cycle extrema. Panel (b) plots the result for all data from Figure 6. The legend gives the numerical values from panel (b). For clarity, only panel (b) shows variability error bars. While these exponents show some variability, we have too few solar cycle extrema to determine if the variations are sufficiently distinct from the overall average behavior in Panel (b) to be significant.

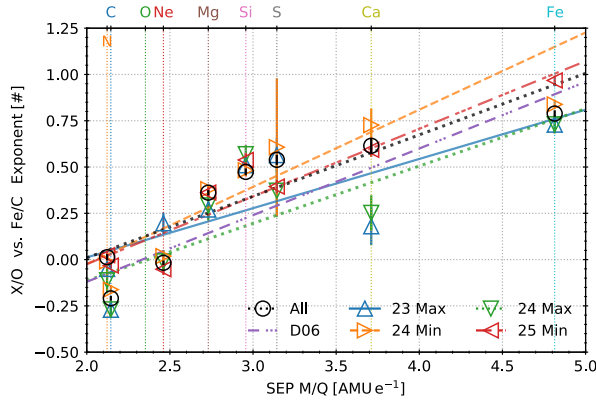


Figure 8. Power law exponents from fits to X/O as a function of Fe/C as a function of M/Q with lines fit to each data subset indicated in the legend. The trend line fits are in Table 3. The *D06* trend is from the equivalent plot for LSEP events by Desai et al. (2006a, Fig. 15). The consistency across these slopes supports the interpretation that LSEP events accelerate a pre-existing ST pool.

5. DISCUSSION

Quiet times are periods when the intensity of the suprathermal population is low. While the suprathermal intensity naturally varies with solar activity, quiet times are nevertheless present throughout the solar cycle (Desai et al. 2006c; Dayeh et al. 2009, 2017; Zel'dovich et al. 2011, 2018, 2021). We study these suprathermal

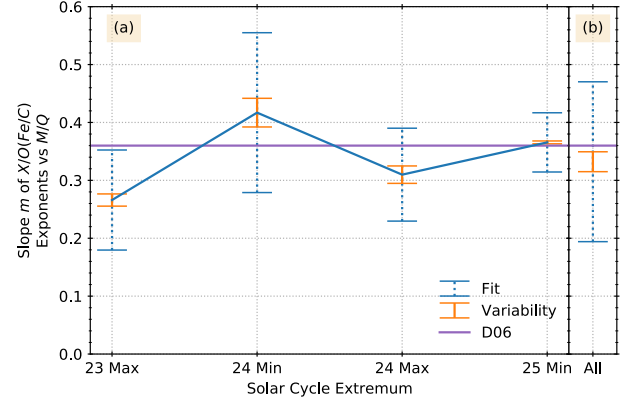


Figure 9. The fractionation trends derived from Figure 8 as a function of (a) solar activity and (b) for all data. This figure shows that ST M/Q fractionation is independent of solar activity.

ions in quiet times across solar activity to characterize their origin.

5.1. Quiet Time Selection and Annual Quiet Hours

The definition of quiet times is still unsettled in the literature and remains *ad hoc*. For example, Zel'dovich et al. (2014, 2018, 2021) select data based on multiple criteria from several instruments across a few spacecraft. In contrast, Desai et al. (2006c); Dayeh et al. (2009, 2017) set thresholds for the Fe or total C through Fe intensity and allow for intensities that report zero counts, i.e. below the instrument detection threshold. Both selection methods rely on one or more manually identified thresholds without a metric to quantify the sensitivity of the results to that selection. As such, quiet time selection necessarily leads to inconsistent labeling of some intervals as quiet or not. For the purposes of this study, a false positive would be a not-quiet interval labeled as quiet and a false negative would be a quiet interval labeled as not-quiet. Quantifying the sensitivity of our result to our quiet time selection criteria provides evidence that such false positives and false negatives do not impact our results.

Section 2.1 utilizes non-linear fitting to identify the QT threshold using the definition described by Dayeh et al. (2017) and provide an accompanying 1σ fit uncertainty. To study the sensitivity of our results to the fit QT threshold, we have calculated 21 uniformly spaced steps over the range ($\text{QT} \pm 1.25\sigma$), centered on the QT fit result. We repeat our analysis for each of these 21 thresholds and, where applicable, representing the variation as the standard deviation of our results as error bars centered on the QT threshold (Alterman & Kasper 2019).

Section 2.2 analyzes each year’s QT threshold and the number of quiet hours, both as a function of time. In general, the QT threshold is weakly correlated in time with SSN ($\rho = 0.51$). However, the number of quiet hours anti-correlates with SSN at the $\rho = -0.95$ level, likely because solar activity drives the occurrence of non-quiet time periods. It is unsurprising that our correlation is stronger than that derived by Dayeh et al. (2009, 2017) because their time series are 13 years⁸ and 17 years⁹, where as ours covers 23 years and longer time series provide additional data with which to characterize any trend or lack there of. In both the case of the QT threshold and the annual number of quiet hours, our results were insensitive to changes in the QT threshold across the $\pm 1.25\sigma$ range.

5.2. Annual Abundances: Suprathermal Sources

Studying 41 CIRs, Mason et al. (2008) infer that energetic particles (EPs) associated in CIRs are drawn from a ST pool composed of solar wind, pickup ions, and SEP remnants. Filwett et al. (2017, 2019) came to similar conclusions about ST ions accelerated by CIRs. Figure 5 (b) shows that normalizing the quiet time X/O to an abundance characteristic of CIRs observed at 0.385 MeV/nuc removes the M/Q-dependence during solar minima.

Studying 72 interplanetary shocks at 0.75 MeV/nuc in solar cycle 23, Desai et al. (2003) suggest that the suprathermal pool from which shocks accelerate energetic particles is composed of 70% GSEP and 30% ISEP remnant material, both from the 5 – 12 MeV/nuc range. Studying 64 LSEP events from solar cycle 23 at 0.38 MeV/nuc, Desai et al. (2006a) suggest that GSEP events are M/Q-fractionated in because of the ambient 0.38 MeV/nuc suprathermal seed population from which they accelerate ions and this suprathermal population is itself primarily drawn from 0.385 MeV/nuc ISEP events. Figure 5 (c) and (d) show that normalizing quiet time X/O to reference abundances from ISEP does not remove the M/Q-dependence, but normalizing it to a GSEP-representative abundance does remove the M/Q-dependence during solar maxima. A mixture of GSEP and ISEP abundances may not be necessary to characterize the quiet time X/O fractionation and Desai et al.’s (2003) observation that suprathermals are composed of 70% GSEP + 30% ISEP remnant particles may be due to their comparison of 0.75 MeV/nuc ions with reference abundances at 5 – 12 MeV/nuc.

⁸ Approximately solar cycle 23

⁹ Approximately cycle 23 into the declining phase of cycle 24.

Suprathermal ions have been observed to suffuse the heliosphere (Tsurutani & Lin 1985; Desai et al. 2003; Wiedenbeck et al. 2003). Long term studies of ST ions across solar cycles 23 and 24 also related differences in ST observations at 1 AU to different solar source regions (Zel’dovich et al. 2018, 2014). That quiet time X/O is most similar to CIRs during solar minima and GSEP abundances during solar maxima further substantiates observations their dominant source changes with solar activity. That these observations are taken during quiet times also substantiates that suprathermals suffice the heliosphere across solar activity. The presence of M/Q-fractionation points to the impact of acceleration on the observed abundances. That the fractionation disappears when normalized to CIR abundances in solar minima and GSEP abundances in solar maxima may imply that SEPs simply decrease in intensity as they spread out through the heliosphere.

5.3. Abundances as a Function of Fe/C: Variability of the Quiet Time Suprathermal Pool

Figure 6 plots each species’ abundance as a function of Fe/C. Unlike analogous observations during ³He-rich ISEP events (Mason et al. 2004), these suprathermal observations are not normally distributed with $\ln(\text{Fe}/\text{C})$. This suggests ISEP events are not the sole source of the suprathermal ions studied in this paper.

Figure 7 plots exponents from the fits to the data in Figure 6 as a function of solar activity. It shows that these exponents may change in a cyclic fashion with solar activity. However, data from further solar cycles are necessary to increase confidence in such an inference.

Figure 8 plots and compares these exponents as a function of M/Q along with the analogous trend for GSEP at 0.38 MeV/nuc events from Desai et al. (2006a). Although the y-intercepts are different, the slopes are consistent across solar activity. As Desai et al.’s (2006a) observations of individual GSEP events cover one solar cycle, our observations suggest that event-to-event variability in their GSEP events is consistent with the long-term variability of ST abundances in quiet times.

Figure 9 takes fits to these exponents as a function of M/Q and plots the resulting slopes as a function of solar activity. It shows that the fit uncertainty is markedly larger than the variability of our results due to QT threshold selection, suggesting that the variability due to QT threshold in Section 2 does not impact our results and they are robust to QT selection threshold.

5.4. Annual Abundance Correlation with SSN: Suprathermal S is low FIP

Reames (2018a,b) argue that the difference in CIR and SEP abundances is a result of the solar source regions

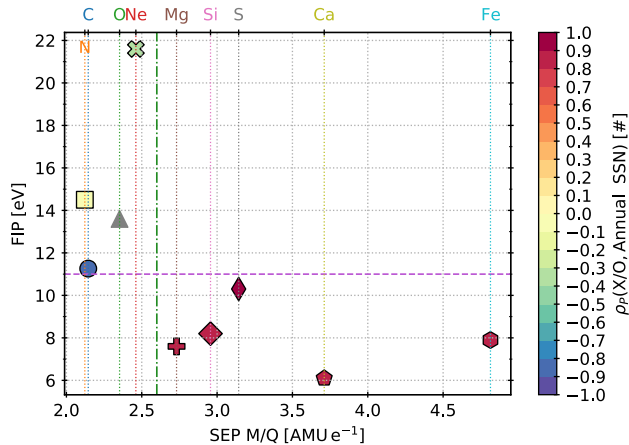


Figure 10. The color-coded correlation coefficient $\rho(X/O, SSN)$ between X/O and SSN as a function of first ionization potential (FIP) and SEP M/Q . Species are indicated on the top axis and a vertical dotted line connects the species label to its M/Q . O is indicated in gray for completeness. The vertical green dash-dotted line indicates $M/Q = 2.6$. The horizontal dashed purple line indicates $FIP = 11$ eV. Considering the impact of acceleration and source region impacts, this figure unexpectedly suggests that S behaves like a low FIP ion even though $FIP = 11$ eV > 10 eV.

from which their ions are released into the heliosphere, in particular the first ionization potential (FIP) effect. The FIP effect is the observation that the abundance of low FIP ions is enhanced relative to their photospheric abundances and high FIP ions are depleted (Laming 2015). Reames (2018b) argue that this low/high FIP separation occurs at ~ 10 eV in SEP events and S is a high FIP SEP element. In particular, Reames (2018a) argues that S behaves like higher FIP elements, of which C is commonly treated as a generic example. As such, we would expect S/O to follow the same temporal variations as C/O .

This work aggregates ST measurements into annual bins, which are orders of magnitude longer in duration than events that accelerate SEPs or the processes related to injection, acceleration, and transport. Table 1 gives the correlation coefficient $\rho(X/O, SSN)$. Given the annual duration of our ST aggregations, these ρ are necessarily related to either how the source from which the ST population is drawn or how the prevalence of different acceleration, injection, and transport mechanisms changes with solar activity. As such, we can use them to test the results of Reames (2018a,b).

Figure 10 plots the color-coded correlation coefficient $\rho(X/O, SSN)$ as a function of SEP M/Q and FIP. Many acceleration and transport processes that impact the solar wind and SEPs depend on M/Q . If changes in

the relative occurrence of these processes drive changes in ρ , then ρ should be ordered by M/Q . If changes in solar source regions drive changes in ρ , then FIP should order it. The clear change in sign ρ at $(M/Q, FIP) \approx (2.6, 11)$ suggests that at least one of M/Q and FIP is significant to long term changes in $\rho(X/O, SSN)$. The question is: which? First, we will show that there is insufficient evidence that ρ depends on M/Q . Then we will discuss that changes in source regions may be related to changes in ρ .

Let us assume that ρ is tied to changes in the prevalence of a rigidity-dependent process. Then ρ should be ordered by M/Q . Two observations indicate this is not the case. (1) Ions with $FIP < 11$ eV all have $\rho > 0.8$, without a clear ordering. (2) High FIP ions show no defined ordering. While only there are only three points high FIP points (C, N, and Ne), we can exclude C/O and its anti-correlation because C is known to be overabundant in the solar wind and CIRs. In other words, C is not necessarily a generic example of high FIP elements. The two remaining points (N and Ne) are insufficient to draw any conclusion about the impact of changes in a rigidity-dependent mechanism on high FIP ions. In short, there is insufficient evidence for an M/Q -dependent process driving ρ .

Let us assume the opposite, that changes in ρ are tied to source region effects at the Sun. The FIP effect yields abundance differences based on how the combination of source region temperatures and height in the solar atmosphere determine when an element ionizes. These temperatures and heights are related to solar source region type (e.g. coronal hole, active region, streamer belt, etc.) from which the ions emanates. Because FIP is tied to source region, this suggests a discrete change in X/O are possible based on the source region driving each abundance. Given the change in ρ 's sign occurs at $FIP \approx 11$ eV and there is no other ordering as a function of M/Q , Figure 10 implies that ρ is driven by source region changes and not the prevalence of any M/Q -dependent process. Absent some other known physical mechanisms, that the change in ρ 's sign occurs at 11 eV implies that S is a low FIP ST ion. Given we have shown that STs are consistent with GSEP and ISEP populations, we must infer that S is low FIP in SEPs—not high FIP (Reames 2018a,b)—and that ST S must originate in the same regions as other low FIP elements like Ca, Fe, Mg, and Si.

6. CONCLUSION

We have developed a method for analyzing long term trends in 0.3 MeV/nuc to 1.28 MeV/nuc ions during quiet times that includes tests for the sensitivity of our

results to our quiet time selection criteria. We refer to these as suprathermals and have shown that the statistical uncertainty in our results dominates any uncertainty due to our quiet time selection criterion. As such, our results and QT threshold proposed by Dayeh et al.'s (2017) are robust.

We have confirmed that the annual number of quiet hours decreases with increasing solar activity (Dayeh et al. 2017). This is likely because the occurrence of phenomena like flares and CMEs that accelerate SEPs increases with SSN. Our results also support prior conclusions that the populations from which ST ions are drawn change with solar activity (Desai et al. 2006c; Dayeh et al. 2009, 2017; Zel'dovich et al. 2011, 2018, 2021). In particular, normalizing quiet time X/O to CIR abundances during solar minima and GSEP abundances during solar maxima removes the trends with M/Q . This suggests that the quiet time suprathermals we observe are remnants of material that was previously accelerated by the dominant energetic particle producer during that epoch, that these energetic particles decay in intensity to the suprathermal regime, and that they are not accelerated out of the solar wind nor decelerated from SEPs. That these observations are made during quiet times further substantiates observations that

suprathermals suffuse the interplanetary medium (Tsurutani & Lin 1985; Desai et al. 2003; Wiedenbeck et al. 2003).

Coincident to these broad findings, our analysis has also revealed that suprathermal S is a low FIP ion. Given that high and low FIP ions are from distinct sources on the Sun, this means that S must be treated like a low FIP ion when tracing SEP events back to their solar sources and modeling SEP acceleration mechanisms.

The authors thank Heather Elliot and Frederic Algrini feedback on this paper. BLA acknowledges NASA grants 80NSSC20K1255 and 80NSSC21K0112. MID acknowledges NASA grants 80NSSC20K1255, 80NSSC21K0112, and 80NSSC21K1572. MAD acknowledges NASA grants 80NSSC19K0079 (LWS), 80NSSC20K0290 (O2R), and contract NNJ15HK11B. GMM acknowledges 80NSSC22K0374.

Software: IPython (Perez & Granger 2007), Jupyter (Kluyver et al. 2016), Matplotlib (Hunter 2007), Numpy (Harris et al. 2020), SciPy (Virtanen et al. 2020), Pandas (McKinney 2010; The Pandas Development Team 2020), Python (Millman & Aivazis 2011; Oliphant 2007)

Table 2. Representative abundances for known populations along with solar cycle extrema. Excluding columns (c), (f), and (l), data matches [Desai et al. \(2006a, Table 3\)](#). Although this paper does not analyze He, it is included in this table for completeness. Where appropriate, energies have been given in the footnotes.

	LSEP ^a	ISEP ^b	CIR ^c	ST in Solar Minima ^d	ST in Solar Maxima ^e
	(a)	(b)	(c)	(d)	(e)
He	75.0 ± 23.6	54 ± 14	273 ± 72
C	0.361 ± 0.012	0.322 ± 0.003	0.760 ± 0.023	0.6134 ± 0.0090	0.4173 ± 0.0042
N	0.119 ± 0.003	0.129 ± 0.002	0.143 ± 0.005	0.1434 ± 0.0037	0.1453 ± 0.0022
O	≡ 1 ± 0.02	≡ 1 ± 0.006	1 ± 0.020	≡ 1	≡ 1
Ne	0.152 ± 0.005	0.261 ± 0.003	0.206 ± 0.009	0.2087 ± 0.0046	0.1938 ± 0.0027
Mg	0.229 ± 0.007	0.37 ± 0.003	0.148 ± 0.006	0.1256 ± 0.0035	0.2497 ± 0.0031
Si	0.235 ± 0.011	0.409 ± 0.004	0.095 ± 0.005	0.0953 ± 0.0031	0.2475 ± 0.0032
S	0.059 ± 0.004	0.118 ± 0.015	0.028 ± 0.002	0.0269 ± 0.0016	0.0715 ± 0.0016
Ca	0.022 ± 0.002	0.06 ± 0.003	0.007 ± 0.001	0.00816 ± 0.00087	0.02830 ± 0.00098
Fe	0.404 ± 0.047	0.95 ± 0.005	0.088 ± 0.007	0.0984 ± 0.0032	0.4298 ± 0.0044
	SSW ^f	FSW ^g	Shocks ^h	Photosphere ⁱ	Corona ^j
	(f)	(g)	(h)	(i)	(j)
He	95.9 ± 28.8	72.7 ± 21.8	44.4 ± 14.4	162 ± 14	126 ± 11
C	0.67 ± 0.067	0.683 ± 0.068	0.368 ± 0.004	0.501 ± 0.058	0.49 ± 0.056
N	0.069 ± 0.021	0.111 ± 0.033	0.142 ± 0.002	0.138 ± 0.022	0.123 ± 0.02
O	≡ 1	≡ 1	≡ 1	≡ 1 ± 0.161	≡ 1 ± 0.161
Ne	0.091 ± 0.027	0.082 ± 0.025	0.172 ± 0.003	0.151 ± 0.021	0.191 ± 0.026
Mg	0.147 ± 0.03	0.105 ± 0.021	0.243 ± 0.004	0.072 ± 0.009	0.224 ± 0.026
Si	0.167 ± 0.034	0.115 ± 0.023	0.213 ± 0.003	0.071 ± 0.007	0.214 ± 0.022
S	0.049 ± 0.01	0.056 ± 0.011	0.05 ± 0.001	0.032 ± 0.008	0.032 ± 0.008
Ca	0.017 ± 0.003	0.0053 ± 0.0014	0.022 ± 0.002	0.005 ± 0.0001	0.013 ± 0.0002
Fe	0.12 ± 0.024	0.092 ± 0.018	0.236 ± 0.01	0.061 ± 0.006	0.186 ± 0.017

^a 0.1 – 10 MeV/nuc with an average value of 0.38 MeV/nuc [Desai et al. \(2006a\)](#)

^b Impulsive SEP from 0.32 – 0.45 MeV/nuc with or \sim 0.385 MeV/nuc ([Mason et al. 2004](#))

^c Coronating Interaction Region from 0.32 – 0.45 MeV/nuc or \sim 0.385 MeV/nuc ([Mason et al. 2008, 1998](#))

^d 0.3 – 1.28 MeV/nuc. Averages taken over solar cycle extrema years in this work.

^e 0.3 – 1.28 MeV/nuc. Averages taken over solar cycle extrema years in this work.

^f Slow Solar Wind; [von Steiger et al. \(2000\)](#), Ca/O from [Wurz et al. \(2003\)](#)

^g Fast Solar Wind; [von Steiger et al. \(2000\)](#), Ca/O from [Wurz et al. \(2003\)](#)

^h 0.1 – 10 MeV/nuc with an average of \sim 0.75 MeV/nuc ([Desai et al. 2003](#))

ⁱ [Lodders \(2003\)](#)

^j [Feldman & Widing \(2003\)](#)

	Slope			Intercept			Cross Correlation		
	Value	Uncertainty	QT	Value	Uncertainty	QT	ρ	p -value	QT
All	0.33	0.140	0.017	-0.65	0.420	0.037	0.89	3.0×10^{-3}	0.002
23-Max	0.27	0.090	0.011	-0.52	0.280	0.041	0.76	2.8×10^{-2}	0.025
24-Min	0.42	0.140	0.025	-0.86	0.400	0.066	0.90	2.3×10^{-3}	0.005
24-Max	0.31	0.080	0.015	-0.73	0.270	0.041	0.82	1.2×10^{-2}	0.031
25-Min	0.37	0.050	0.002	-0.76	0.170	0.010	0.94	5.0×10^{-4}	0.007
LESP (D06)	0.36	0.002	...	-0.84	0.007	...	0.97	3.4×10^{-6}	...

Table 3. Parameters from the linear fits in Figure 8 along with the correlation coefficient with SEP M/Q and the associated p -value. QT columns give the variability over the QT thresholds, which are smaller than the statistical uncertainty for the QT threshold derived in Section 2.

Table 4. Annual abundances normalized to oxygen (X/O) and their uncertainties (Uncert) from Figure 4. All data from ACE/ULEIS over the energy range 0.3 MeV/nuc to 1.28 MeV/nuc.

Year	C		N		Ne		Mg		Si		S		Ca		Fe	
	X/O	Uncert	X/O	Uncert	X/O	Uncert	X/O	Uncert	X/O	Uncert	X/O	Uncert	X/O	Uncert	X/O	Uncert
1998	0.51	0.02	0.16	0.009	0.2	0.01	0.22	0.01	0.181	0.01	0.051	0.005	0.026	0.004	0.31	0.01
1999	0.43	0.01	0.155	0.006	0.205	0.007	0.257	0.008	0.257	0.008	0.075	0.004	0.029	0.002	0.52	0.01
2000	0.41	0.01	0.157	0.007	0.211	0.009	0.27	0.01	0.31	0.01	0.096	0.006	0.039	0.004	0.53	0.02
2001	0.4	0.01	0.139	0.007	0.196	0.008	0.251	0.01	0.229	0.009	0.066	0.005	0.026	0.003	0.42	0.01
2002	0.39	0.01	0.14	0.007	0.178	0.008	0.24	0.01	0.23	0.01	0.078	0.006	0.028	0.003	0.39	0.01
2003	0.49	0.01	0.159	0.007	0.187	0.008	0.22	0.009	0.215	0.009	0.063	0.004	0.029	0.003	0.38	0.01
2004	0.48	0.01	0.14	0.007	0.201	0.008	0.236	0.009	0.212	0.009	0.057	0.004	0.029	0.003	0.4	0.01
2005	0.56	0.01	0.154	0.005	0.197	0.006	0.164	0.006	0.154	0.006	0.047	0.003	0.014	0.002	0.178	0.006
2006	0.62	0.02	0.15	0.008	0.207	0.01	0.166	0.008	0.135	0.008	0.044	0.004	0.023	0.003	0.25	0.01
2007	0.65	0.02	0.136	0.007	0.22	0.009	0.126	0.007	0.098	0.006	0.023	0.003	0.005	0.001	0.097	0.006
2008	0.62	0.02	0.143	0.009	0.19	0.01	0.122	0.008	0.092	0.007	0.024	0.004	0.009	0.002	0.094	0.007
2009	0.52	0.04	0.18	0.02	0.24	0.02	0.12	0.02	0.07	0.01	0.036	0.009	0.023	0.007	0.14	0.02
2010	0.5	0.02	0.14	0.007	0.186	0.008	0.166	0.008	0.159	0.008	0.049	0.004	0.015	0.002	0.236	0.01
2011	0.48	0.01	0.146	0.006	0.206	0.008	0.24	0.008	0.215	0.008	0.062	0.004	0.024	0.003	0.38	0.01
2012	0.41	0.01	0.138	0.006	0.176	0.007	0.242	0.008	0.238	0.008	0.061	0.004	0.028	0.003	0.35	0.01
2013	0.42	0.01	0.141	0.006	0.195	0.007	0.239	0.008	0.25	0.008	0.07	0.004	0.028	0.003	0.46	0.01
2014	0.39	0.01	0.146	0.006	0.187	0.007	0.264	0.009	0.274	0.009	0.08	0.005	0.03	0.003	0.45	0.01
2015	0.46	0.01	0.152	0.007	0.188	0.008	0.219	0.009	0.201	0.008	0.066	0.005	0.026	0.003	0.31	0.01
2016	0.59	0.02	0.144	0.006	0.188	0.008	0.18	0.007	0.175	0.008	0.042	0.003	0.016	0.002	0.252	0.009
2017	0.61	0.02	0.152	0.008	0.231	0.01	0.16	0.008	0.139	0.007	0.035	0.004	0.012	0.002	0.18	0.009
2018	0.61	0.02	0.139	0.008	0.203	0.01	0.105	0.007	0.079	0.006	0.023	0.003	0.007	0.002	0.06	0.005
2019	0.53	0.03	0.15	0.01	0.21	0.02	0.11	0.01	0.09	0.01	0.028	0.006	0.012	0.004	0.13	0.01

REFERENCES

- Allen, R. C., Ho, G. C., & Mason, G. 2019, *The Astrophysical Journal*, 883, L10, doi: [10.3847/2041-8213/ab3f2f](https://doi.org/10.3847/2041-8213/ab3f2f)
- Alterman, B. L., & Kasper, J. C. 2019, *The Astrophysical Journal*, 879, L6, doi: [10.3847/2041-8213/ab2391](https://doi.org/10.3847/2041-8213/ab2391)
- Alterman, B. L., Kasper, J. C., Leamon, R. J., & McIntosh, S. W. 2021, *Solar Physics*, 296, 67, doi: [10.1007/s11207-021-01801-9](https://doi.org/10.1007/s11207-021-01801-9)
- Blum, P. W., & Fahr, H. J. 1970, *Astronomy and Astrophysics*, 4, 280, <https://ui.adsabs.harvard.edu/abs/1970A&A.....4..280B>
- Chotoo, K., Schwadron, N. A., Mason, G., et al. 2000, *Journal of Geophysical Research: Space Physics*, 105, 23107, doi: [10.1029/1998ja000015](https://doi.org/10.1029/1998ja000015)
- Dayeh, M. A., Desai, M., Dwyer, J. R., et al. 2009, *Astrophysical Journal*, 693, 1588, doi: [10.1088/0004-637X/693/2/1588](https://doi.org/10.1088/0004-637X/693/2/1588)
- Dayeh, M. A., Desai, M., Mason, G., Ebert, R. W., & Farahat, A. 2017, *The Astrophysical Journal*, 835, 155, doi: [10.3847/1538-4357/835/2/155](https://doi.org/10.3847/1538-4357/835/2/155)
- Desai, M., & Giacalone, J. 2016, *Living Reviews in Solar Physics*, 13, 3, doi: [10.1007/s41116-016-0002-5](https://doi.org/10.1007/s41116-016-0002-5)
- Desai, M., & Mason, G. 2001, *The Astrophysical Journal*, 553, 89, <http://iopscience.iop.org/1538-4357/553/1/L89>
- Desai, M., Mason, G., Dwyer, J. R., et al. 2003, *The Astrophysical Journal*, 588, 1149, doi: [10.1086/374310](https://doi.org/10.1086/374310)
- Desai, M., Mason, G., Gold, R. E., et al. 2007, *Space Science Reviews*, 130, 243, doi: [10.1007/s11214-007-9219-x](https://doi.org/10.1007/s11214-007-9219-x)
- . 2006a, *The Astrophysical Journal*, 649, 470, doi: [10.1086/505649](https://doi.org/10.1086/505649)
- Desai, M., Mason, G., Mazur, J. E., & Dwyer, J. R. 2006b, *Space Science Reviews*, 124, 261, doi: [10.1007/s11214-006-9109-7](https://doi.org/10.1007/s11214-006-9109-7)
- . 2006c, *The Astrophysical Journal*, 645, L81, doi: [10.1086/505935](https://doi.org/10.1086/505935)
- Desai, M., Mason, G., Wiedenbeck, M. E., et al. 2004, *The Astrophysical Journal*, 611, 1156, doi: [10.1086/422211](https://doi.org/10.1086/422211)
- Drake, J. F., Swisdak, M., & Fermo, R. 2013, *Astrophysical Journal Letters*, 763, 1, doi: [10.1088/2041-8205/763/1/L5](https://doi.org/10.1088/2041-8205/763/1/L5)
- Ebert, R. W., Dayeh, M. A., Desai, M., & Mason, G. 2012, *Astrophysical Journal*, 749, doi: [10.1088/0004-637X/749/1/73](https://doi.org/10.1088/0004-637X/749/1/73)
- Fahr, H. J., Chashei, I. V., & Siewert, M. 2012, *Astronomy & Astrophysics*, 537, 1, doi: [10.1051/0004-6361/201117503](https://doi.org/10.1051/0004-6361/201117503)
- Feldman, U., & Widing, K. G. 2003, *Space Science Reviews*, 107, 665, doi: [10.1023/A:1026103726147](https://doi.org/10.1023/A:1026103726147)
- Feldman, W. C., Asbridge, J. R., Bame, S. J., & Kearney, P. D. 1974, *Journal of Geophysical Research*, 79, 1808, doi: [10.1029/ja079i013p01808](https://doi.org/10.1029/ja079i013p01808)
- Filwett, R. J., Desai, M., Dayeh, M. A., & Broiles, T. W. 2017, *The Astrophysical Journal*, 838, 23, doi: [10.3847/1538-4357/aa5ca9](https://doi.org/10.3847/1538-4357/aa5ca9)
- Filwett, R. J., Desai, M., Ebert, R. W., & Dayeh, M. A. 2019, *The Astrophysical Journal*, 876, 88, doi: [10.3847/1538-4357/ab12cf](https://doi.org/10.3847/1538-4357/ab12cf)
- Fisk, L. A., & Gloeckler, G. 2006, *The Astrophysical Journal*, 640, L79, doi: [10.1086/503293](https://doi.org/10.1086/503293)
- . 2008, *The Astrophysical Journal*, 686, 1466, doi: [10.1086/591543](https://doi.org/10.1086/591543)
- . 2012, *AIP Conference Proceedings*, 1436, 116, doi: [10.1063/1.4723598](https://doi.org/10.1063/1.4723598)
- . 2014, *Journal of Geophysical Research: Space Physics*, 119, 8733, doi: [10.1002/2014JA020426](https://doi.org/10.1002/2014JA020426)
- Fisk, L. A., & Lee, M. A. 1980, *The Astrophysical Journal*, 237, 620, doi: [10.1086/157907](https://doi.org/10.1086/157907)
- Gloeckler, G., Fisk, L. A., Mason, G., & Hill, M. E. 2008, *AIP Conference Proceedings*, 1039, 367, doi: [10.1063/1.2982473](https://doi.org/10.1063/1.2982473)
- Harris, C. R., Millman, K. J., van der Walt, S. J., et al. 2020, *Nature*, 585, 357, doi: [10.1038/s41586-020-2649-2](https://doi.org/10.1038/s41586-020-2649-2)
- Holzer, T. E., & Axford, W. I. 1971, *Journal of Geophysical Research*, 76, 6965, doi: [10.1029/JA076i028p06965](https://doi.org/10.1029/JA076i028p06965)
- Hovestadt, D., Klecker, B., Scholer, M., & Gloeckler, G. 1984a, *The Astrophysical Journal*, 281, 463, doi: [10.1086/162118](https://doi.org/10.1086/162118)
- Hovestadt, D., Klecker, B., Scholer, M., Gloeckler, G., & Ipavich, F. M. 1984b, *The Astrophysical Journal*, 282, L39, doi: [10.1086/184300](https://doi.org/10.1086/184300)
- Hunter, J. D. 2007, *Computing in Science & Engineering*, 9, 90, doi: [10.1109/MCSE.2007.55](https://doi.org/10.1109/MCSE.2007.55)
- Jones, F. C., & Ellison, D. C. 1991, *Space Science Reviews*, 58, 259, doi: [10.1007/BF01206003](https://doi.org/10.1007/BF01206003)
- Kahler, S. W., & Ling, A. G. 2019, *The Astrophysical Journal*, 872, 89, doi: [10.3847/1538-4357/aafb03](https://doi.org/10.3847/1538-4357/aafb03)
- Kluyver, T., Ragan-kelley, B., Pérez, F., et al. 2016, *Positioning and Power in Academic Publishing: Players, Agents and Agendas*, 87, doi: [10.3233/978-1-61499-649-1-87](https://doi.org/10.3233/978-1-61499-649-1-87)
- Laming, J. M. 2015, *Living Reviews in Solar Physics*, 12, doi: [10.1007/lrsp-2015-2](https://doi.org/10.1007/lrsp-2015-2)
- Lario, D., Berger, L., Decker, R. B., et al. 2019, *The Astronomical Journal*, 158, 12, doi: [10.3847/1538-3881/ab1e49](https://doi.org/10.3847/1538-3881/ab1e49)
- Lodders, K. 2003, *The Astrophysical Journal*, 591, 1220, <http://stacks.iop.org/0004-637X/591/i=2/a=1220>

- Mason, G., & Gloeckler, G. 2012in , 241–251, doi: [10.1007/s11214-010-9741-0](https://doi.org/10.1007/s11214-010-9741-0)
- Mason, G., Mazur, J. E., & Dwyer, J. R. 1999, *The Astrophysical Journal*, 525, L133, doi: [10.1086/312349](https://doi.org/10.1086/312349)
- Mason, G., Mazur, J. E., Dwyer, J. R., et al. 2004, *The Astrophysical Journal*, 606, 555, doi: [10.1086/382864](https://doi.org/10.1086/382864)
- Mason, G., Mazur, J. E., Dwyer, J. R., Reames, D. V., & von Roseninge, T. T. 1997, *The Astrophysical Journal*, 486, L149, doi: [10.1086/310845](https://doi.org/10.1086/310845)
- Mason, G., Nitta, N. V., Wiedenbeck, M. E., & Innes, D. E. 2016, *The Astrophysical Journal*, 823, 138, doi: [10.3847/0004-637x/823/2/138](https://doi.org/10.3847/0004-637x/823/2/138)
- Mason, G., Gold, R. E., Krimigis, S. M., et al. 1998, *Space Science Reviews*, 86, 409, doi: [10.1023/A:1005079930780](https://doi.org/10.1023/A:1005079930780)
- Mason, G., Wiedenbeck, M. E., Miller, J. A., et al. 2002, *The Astrophysical Journal*, 574, 1039, doi: [10.1086/341112](https://doi.org/10.1086/341112)
- Mason, G., Leske, R., Desai, M., et al. 2008, *The Astrophysical Journal*, 678, 1458, doi: [10.1086/533524](https://doi.org/10.1086/533524)
- McIntosh, S. W., & Leamon, R. J. 2017, *Frontiers in Astronomy and Space Sciences*, 4, 1, doi: [10.3389/fspas.2017.00004](https://doi.org/10.3389/fspas.2017.00004)
- McIntosh, S. W., Wang, X., Leamon, R. J., et al. 2014, *Astrophysical Journal*, 792, doi: [10.1088/0004-637X/792/1/12](https://doi.org/10.1088/0004-637X/792/1/12)
- McIntosh, S. W., Leamon, R. J., Krista, L. D., et al. 2015, *Nature Communications*, 6, 1, doi: [10.1038/ncomms7491](https://doi.org/10.1038/ncomms7491)
- McKinney, W. 2010, in *Proceedings of the 9th Python in Science Conference*, ed. S. van der Walt & J. Millman, 56–61, doi: [10.25080/Majora-92bf1922-00a](https://doi.org/10.25080/Majora-92bf1922-00a)
- Mewaldt, R. 2001, in *AIP Conference Proceedings*, Vol. 598 (AIP), 165–170, doi: [10.1063/1.1433995](https://doi.org/10.1063/1.1433995)
- Mewaldt, R., Mason, G., & Cohen, C. M. 2012, *AIP Conference Proceedings*, 1500, 128, doi: [10.1063/1.4768755](https://doi.org/10.1063/1.4768755)
- Millman, K. J., & Aivazis, M. 2011, *Computing in Science & Engineering*, 13, 9, doi: [10.1109/MCSE.2011.36](https://doi.org/10.1109/MCSE.2011.36)
- Möbius, E., Rucinski, D., Hovestadt, D., & Klecker, B. 1995, *Astronomy & Astrophysics*, 304, 505. <http://adsabs.harvard.edu/abs/1995A&A...304..505M>
- Oliphant, T. E. 2007, *Computing in Science & Engineering*, 9, 10, doi: [10.1109/MCSE.2007.58](https://doi.org/10.1109/MCSE.2007.58)
- Perez, F., & Granger, B. E. 2007, *Computing in Science & Engineering*, 9, 21, doi: [10.1109/MCSE.2007.53](https://doi.org/10.1109/MCSE.2007.53)
- Reames, D. V. 1995, *Advances in Space Research*, 15, 41, doi: [10.1016/0273-1177\(94\)00018-V](https://doi.org/10.1016/0273-1177(94)00018-V)
- . 1999, *Space Science Review*, 90, 413–491, doi: [10.1023/A:1005105831781](https://doi.org/10.1023/A:1005105831781)
- . 2018a, *Space Science Reviews*, 214, doi: [10.1007/s11214-018-0495-4](https://doi.org/10.1007/s11214-018-0495-4)
- . 2018b, *Solar Physics*, 293, doi: [10.1007/s11207-018-1369-3](https://doi.org/10.1007/s11207-018-1369-3)
- Reames, D. V., Meyer, J. P., & von Roseninge, T. T. 1994, *The Astrophysical Journal Supplement Series*, 90, 649, doi: [10.1086/191887](https://doi.org/10.1086/191887)
- Richardson, I. G. 2004, *Space Science Reviews*, 111, 267, doi: [10.1023/B:SPAC.0000032689.52830.3e](https://doi.org/10.1023/B:SPAC.0000032689.52830.3e)
- SILSO World Data Center. 2020
- The Pandas Development Team. 2020, *pandas-dev/pandas: Pandas*, doi: [10.5281/zenodo.3509134](https://doi.org/10.5281/zenodo.3509134)
- Tsurutani, B. T., & Lin, R. P. 1985, *Journal of Geophysical Research*, 90, 1, doi: [10.1029/JA090iA01p00001](https://doi.org/10.1029/JA090iA01p00001)
- Vanlommel, P., Cugnon, P., Van Der Linden, R. A. M., Berghmans, D., & Clette, F. 2005, *Solar Physics*, 224, 113, doi: [10.1007/s11207-005-6504-2](https://doi.org/10.1007/s11207-005-6504-2)
- Virtanen, P., Gommers, R., Oliphant, T. E., et al. 2020, *Nature Methods*, 17, 261, doi: [10.1038/s41592-019-0686-2](https://doi.org/10.1038/s41592-019-0686-2)
- von Roseninge, T. T., Barbier, L. M., Karsch, J., et al. 1995, *Space Science Reviews*, 71, 155, doi: [10.1007/BF00751329](https://doi.org/10.1007/BF00751329)
- von Steiger, R., Schwadron, N. A., Fisk, L. A., et al. 2000, *Journal of Geophysical Research: Space Physics*, 105, 27217, doi: [10.1029/1999ja000358](https://doi.org/10.1029/1999ja000358)
- Webb, D. F., & Howard, R. A. 1994, *Journal of Geophysical Research*, 99, 4201, doi: [10.1029/93JA02742](https://doi.org/10.1029/93JA02742)
- Wiedenbeck, M. E., Mason, G. M., Christian, E. R., et al. 2003, *AIP Conference Proceedings*, 679, 652, doi: [10.1063/1.1618679](https://doi.org/10.1063/1.1618679)
- Wurz, P., Bochsler, P., Paquette, J. A., & Ipavich, F. M. 2003, *The Astrophysical Journal*, 583, 489, doi: [10.1086/344834](https://doi.org/10.1086/344834)
- Zank, G. P., Le Roux, J. A., Webb, G. M., Dosch, A., & Khabarova, O. 2014, *Astrophysical Journal*, 797, doi: [10.1088/0004-637X/797/1/28](https://doi.org/10.1088/0004-637X/797/1/28)
- Zank, G. P., Li, G., Florinski, V., et al. 2006, *Journal of Geophysical Research: Space Physics*, 111, 1, doi: [10.1029/2005JA011524](https://doi.org/10.1029/2005JA011524)
- Zel'dovich, M. A., Kecskeméty, K., & Logachev, Y. I. 2021, *Monthly Notices of the Royal Astronomical Society*, 502, 2961, doi: [10.1093/mnras/staa4029](https://doi.org/10.1093/mnras/staa4029)
- Zel'dovich, M. A., Logachev, Y. I., & Kecskeméty, K. 2018, *Solar Physics*, 293, doi: [10.1007/s11207-017-1170-8](https://doi.org/10.1007/s11207-017-1170-8)
- Zel'dovich, M. A., Logachev, Y. I., & Surova, G. M. 2011, *Astronomy Reports*, 55, 374, doi: [10.1134/S1063772911020090](https://doi.org/10.1134/S1063772911020090)
- Zel'dovich, M. A., Logachev, Y. I., Surova, G. M., & Kecskeméty, K. 2014, *Astronomy Reports*, 58, 399, doi: [10.1134/S1063772914050072](https://doi.org/10.1134/S1063772914050072)

Zhao, L., Landi, E., & Gibson, S. E. 2013, The
Astrophysical Journal, 773, 157,
doi: [10.1088/0004-637X/773/2/157](https://doi.org/10.1088/0004-637X/773/2/157)